JOURNAL OF GEOPHYSICAL RESEARCH, VOL. ???, XXXX, DOI:10.1029/,

Shocklets, SLAMS, and field-aligned ion beams in the terrestrial foreshock

L.B. Wilson III,[1] A. Koval,[5,1] D.G. Sibeck,[1] A. Szabo,[1] C.A. Cattell,[2] J.C. Kasper[3] B.A. Maruca[3] M. Pulupa[4] C.S. Salem[4] M. Wilber[4]

Abstract. We present Wind spacecraft observations of ion distributions showing field-aligned beams (FABs) and large-amplitude magnetic fluctuations composed of a series of shocklets and short large-amplitude magnetic structures (SLAMS). The FABs are found to have $T_b \sim$ 80-850 eV, $V_b/V_{sw} \sim$ 1.3-2.4, $T_{\perp,b}/T_{\parallel,b} \sim$ 1-8, and $n_b/n_o \sim$ 0.2-11%. Saturation amplitudes for ion/ion resonant and non-resonant instabilities are too small to explain the observed SLAMS amplitudes. We show two examples where groups of SLAMS can act like a local quasi-perpendicular shock reflecting ions to produce the FABs, a scenario distinct from the more-common production at the quasi-perpendicular bow shock. The SLAMS exhibit a foot-like magnetic enhancement with a leading magnetosonic whistler train, consistent with previous observations. Strong ion and electron heating are observed within the series of shocklets and SLAMS with temperatures increasing by factors $\gtrsim$5 and $\gtrsim$3, respectively. Both the core and halo electron components show strong perpendicular heating inside the feature. [Date: 10/09/2012]

1. Introduction

Collisionless shock waves are a ubiquitous phenomena in space plasmas and are known to produce several different populations of reflected ion species, including: (1) field-aligned beams (FABs) [*e.g. Greenstadt*, 1976; *Bonifazi and Moreno*, 1981a, b], (2) intermediate ions [*e.g. Paschmann et al.*, 1979], (3) diffuse ions [*e.g. Gosling et al.*, 1978], (4) gyrating ions [*e.g. Meziane et al.*, 1997], and (5) gyrophase-bunched ions [*e.g. Gurgiolo et al.*, 1981]. The first three types are nearly gyrotropic and only distinguished by their pitch-angle distributions [*e.g. Paschmann et al.*, 1981]. The difference between gyrating and gyrophase-bunched ions has been defined by their gyrotropy [*e.g. Fuselier et al.*, 1986] and relative distance from the terrestrial bow shock [*e.g. Meziane et al.*, 2001]. These ion distributions have been examined in detail [*e.g. Paschmann et al.*, 1981; *Bale et al.*, 2005; *Eastwood et al.*, 2005, *and references therein*] and all the ion species have been observed to be spatially well separated [*e.g. Meziane et al.*, 2011]. We will focus on FABs of finite spatial extent herein.

The properties of reflected ion distributions depend strongly upon the shock geometry where the ion reflected from the shock surface. The shock normal angle, θ_{Bn}, is defined by the angle between the the average upstream magnetic field and the local shock normal vector. The shock geometry is called quasi-perpendicular(-parallel) when θ_{Bn} >(<) 45°. Early observations [*Greenstadt*, 1976] suggested that FABs had their origin on field lines connected to a quasi-perpendicular portion of the bow shock. Later studies found consistent results, namely that FABs are typically observed upstream of the quasi-perpendicular bow shock [*e.g. Fuselier*, 1995]. However, theory suggests that specular reflection under quasi-parallel geometry results in a guiding center velocity directed upstream [*e.g. Gosling et al.*, 1982], which has been supported by observations [*e.g. Thomsen et al.*, 1990].

FABs are primarily composed of protons streaming along the ambient magnetic field away from the bow shock with temperatures (T_b) ~80-600 eV, densities (n_b) 1-10% of the ambient solar wind density (n_o), and beam speeds up to 5 times the solar wind speed (V_{sw}) [*Bonifazi and Moreno*, 1981a, b; *Paschmann et al.*, 1981]. FABs often have strong temperature anisotropies with $T_{\perp,b}/T_{\parallel,b} \gtrsim$ 4-9 [*Paschmann et al.*, 1981]. They are typically observed in the absence of or near large magnetic fluctuations, but not simultaneously with these waves [*Kis et al.*, 2007; *Meziane et al.*, 2011]. Note that *Meziane et al.* [2004] observed FABs simultaneously with gyrating ions near the ultra-low frequency (ULF) wave boundary, due to finite gyroradius effects.

The terrestrial foreshock on the quasi-parallel side has a broad spectrum of large amplitude waves. This spectrum consists of transverse Alfvénic waves, right-hand polarized (in plasma frame) ULF waves near the ion gyrofrequency (f_{ci}), compressional magnetosonic waves [*Hoppe and Russell*, 1983], magnetosonic-whistler mode waves [*Hoppe et al.*, 1981], and an ensemble of higher frequency (f > 5-10 Hz) waves up to the electron plasma frequency (f_{pe}) [*e.g. Briand*, 2009, *and references therein*]. We will focus on two specific types of waves in the foreshock, shocklets [*Hoppe et al.*, 1981] and short large-amplitude magnetic structures (SLAMS) [*Schwartz et al.*, 1992]. Both types are magnetosonic in nature [*Hoppe et al.*, 1981; *Mann et al.*, 1994; *Behlke et al.*, 2003; *Hellinger and Mangeney*, 1999], which means magnetic fluctuations, δB, are in phase with density fluctuations, δn. The magnetosonic nature of shocklets and SLAMS causes them to dispersively radiate higher frequency electromagnetic whistler precursor waves as they steepen and they are always observed simultaneously with diffuse ion distributions [*e.g. Wilson III et al.*, 2009, *and references therein*]. Hybrid simulations found that SLAMS could be produced by electromagnetic ion/ion beam instabilities [*Onsager et al.*, 1991; *Akimoto et al.*, 1993; *Dubouloz and*

[1]NASA Goddard Space Flight Center, Greenbelt, Maryland, USA.
[2]School of Physics and Astronomy, University of Minnesota, Minneapolis, Minnesota, USA.
[3]Harvard-Smithsonian Center for Astrophysics, Harvard University, Cambridge, Massachusetts, USA.
[4]Space Sciences Lab, University of California at Berkeley, Berkeley, California, USA.
[5]Goddard Planetary Heliophysics Institute, University of Maryland Baltimore County, Baltimore, Maryland, USA.

0148-0227/12/$9.00

Scholer, 1995; *Hellinger and Mangeney*, 1999]. Particle-In-Cell (PIC) simulations, however, have found that shocklets and SLAMS can result from a nonlinear interaction between gradients in the diffuse ion densities and the ULF wave field [*e.g. Scholer et al.*, 2003; *Tsubouchi and Lembège*, 2004]. The exact nature of SLAMS formation is still unknown but it clearly requires nonlinear instabilities.

SLAMS have been found to have wave vectors directed upstream away from the bow shock. Observations have shown that their phase speed is less than the solar wind speed but ∼1-6 V_A [*e.g. Mann et al.*, 1994], where V_A is the Alfvén speed. Multi-spacecraft studies have found their convection speed (relative to the bow shock) to decrease with increasing amplitude [*e.g. Schwartz et al.*, 1992; *Mann et al.*, 1994] and decreasing distance to the bow shock [*e.g. Mann et al.*, 1994; *Blanco-Cano*, 2010]. This implies that larger amplitude SLAMS can stand against the incident solar wind flow. Simulations have shown their wave vectors become more aligned with the local shock normal with decreasing distance to the shock [*e.g. Dubouloz and Scholer*, 1995], which supports the predictions of *Schwartz and Burgess* [1991]. *Lucek et al.* [2002] found that shocklets and ULF waves have larger scale sizes than SLAMS. Later, *Lucek et al.* [2004, 2008] determined that SLAMS scale sizes parallel to the shock normal were $\gtrsim$1000 km and ∼1300 km parallel to the shock surface. They also found that the gradient scale length of the magnetic field was ∼100 km. SLAMS and shocklets are more easily differentiated by their relative amplitudes. Shocklets exhibit weak magnetic compression with $\delta B/B_o \lesssim 2$, while SLAMS are much stronger with $\delta B/B_o > 2$ and often exceeding a factor of 4.

Previous studies have found FABs near SLAMS, but instrumental limitations prevented an examination of the evolution of the ion distributions across the SLAMS [*Schwartz et al.*, 1992; *Wilkinson et al.*, 1993]. *Wilkinson et al.* [1993] concluded that the SLAMS were generated by a right-hand resonant ion/ion instability [*e.g. Onsager et al.*, 1991; *Akimoto et al.*, 1993]. They also concluded that the observed ion beams were most likely reflected off of a locally non-planar surface, like the SLAMS, but they do not exclude the bow shock as a source. *Giacalone et al.* [1993] found an increase in suprathermal ion pressure associated with SLAMS convecting back toward the bow shock. The pressure increase was observed on the side of the SLAMS facing the bow shock, suggesting the structures were preventing back-streaming suprathermal ions from escaping farther upstream. These results coupled with observations showing gradient scale lengths ∼100 km support the hypothesis by *Mann et al.* [1994] that SLAMS can act as efficient particle mirrors.

In this paper we report the first high time resolution observations of the evolution of FABs through large amplitude magnetic fluctuations, identified as shocklets and SLAMS, in the terrestrial foreshock. The ion beams are more intense on the upstream(sunward) side of the SLAMS, suggesting a local source. This is the first reported occurrence of a secondary mechanism for FAB production. The paper is organized as follows: Section 2 discusses the data sets and analysis techniques, Section 3.1 provides an overview of relevant parameters, Section 3.2 summarizes the particle distribution observations, Section 3.3 justifies our conclusion that the group of SLAMS produce the FABs, and Section 4 presents our conclusions.

2. Data Sets and Analysis

The magnetic field was obtained from the Wind dual, triaxial fluxgate magnetometers [*Lepping et al.*, 1995] sampled at ∼11 samples/s. Full 4π steradian low energy (<30 keV) ion and electron distributions were obtained from the Wind/3DP EESA and PESA particle detectors [*Lin et al.*, 1995]. For more details about the analysis of data from the 3DP instrument, see *Wilson III et al.* [2010]. The solar wind velocity ($\mathbf{V}_{sw}$), ion thermal speed (V_{Ti}, where ${V_{Ts}}^2 = 2k_B T_s/m_s$ for species s), and average ion temperature (T_i) were determined with the 3DP PESA Low and SWE Faraday Cups (FCs) [*Ogilvie et al.*, 1995]. Absolute electron densities were determined from the plasma line in the WAVES thermal noise receiver (TNR) instrument *Bougeret et al.* [1995] and used as an estimate of the solar wind ion density (n_o).

To compare our observations to theory for the growth of SLAMS through a right-hand resonant ion/ion beam instability [*e.g. Akimoto et al.*, 1993], we fit the FABs to bi-Maxwellians to determine estimates of the density (n_b), the temperature (T_b) or thermal speed (V_{Tb}), and beam speed (V_b). The maximum growth rate (γ_{max}) for this instability is proportional to $(n_b/n_o)^{1/3}\ \Omega_{ci}$, where Ω_{ci} is the ion cyclotron frequency. The corresponding wave number (k_{max}) normalized by the ratio V_A/Ω_{ci}, is proportional to V_{Ti}/V_b, where V_A is the Alfvén speed. The corresponding real part of the frequency (ω_{rmax}) is proportional to $(V_{Ti}/V_A - 1)\ \Omega_{ci}$, which can be related to the period of the SLAMS. The FABs are all observed when $V_b/V_A \gg 1$. Under these conditions, the saturation amplitude of the right-hand resonant (and non-resonant) ion/ion beam instability is given by $\delta B/B_o \sim (n_b/2n_o)^{1/2}(V_b/V_A)$ [*e.g. Gary*, 1991]. We will use these relationships to compare observations with theory.

The wave vector, $\mathbf{k}$, and the polarization with respect to the quasi-static magnetic field were determined using Minimum Variance Analysis (MVA) [*Khrabrov and Sonnerup*, 1998]. The details of this technique are discussed in *Wilson III et al.* [2009]. The uncertainties of this analysis are described by *Khrabrov and Sonnerup* [1998]. We calculated the angles between the wave vector and the local magnetic field (θ_{kB}) and the solar wind velocity (θ_{kV}). This analysis was only applied to the shocklets, SLAMS, whistler precursors, and foreshock fluctuations.

We used two methods to determine the bow shock normal vector. The first involved the use of the Rankine-Hugoniot conservation relations [*e.g. Koval and Szabo*, 2008] with the parameters observed at the last crossing of the bow shock. From this we derive a single shock normal vector. The second method involved projecting the local smoothed magnetic field vector onto the surface of a model bow shock [*Slavin and Holzer*, 1981]. Once we determined the shock normal vector, we were able to calculate the shock normal angle, θ_{Bn}. Due to the known errors inherent in each model and the dynamic nature of the bow shock, we use each shock normal estimate as a qualitative reference to assist in our analysis.

3. Observations

3.1. Foreshock Observation Overview

Figure 1 shows the trajectory of the Wind spacecraft in the XY-GSE plane for the two dates examined. The projection of the average magnetic field vector in the foreshock (green arrows) was determined by averaging the magnetic field for the time period between the foreshock structures (blue asterisks) and the foreshock boundary (green square). The projection of the average interplanetary magnetic field (IMF, red arrows) was determined by averaging the smoothed magnetic field for the time period upstream of the foreshock boundary, which was 20:12-23:59 UT for 2000-04-10 and 14:10-17:10 UT for 2002-08-10. We also included the projection of the model magnetopause and bow shock locations, where we adjusted the model parameters to match the observed crossings along the shown trajectories.

The foreshock structures, identified as groups of shocklets

and SLAMS, were located at a GSE position of $\sim$<+13.6, -12.4, +0.02> R_E for the 2000-04-10 event (left panel) and $\sim$<+13.8, -3.0, +0.4> R_E for the 2002-08-10 event (right panel). These positions correspond to distances of $\sim$1.4 R_E ($\sim$60 ion inertial lengths, c/ω_{pi}) and $\sim$2.4 R_E ($\sim$220 c/ω_{pi}) from the last bow shock crossings, respectively. Therefore, we needed to determine whether these structures were simply due to an expansion of or close encounter with the terrestrial bow shock.

To exclude the possibility of a bow shock expansion, we examined data from the ACE, GOES 8 and 10, and Interball spacecraft (courtesy of CDAWeb). We found no transient sudden reduction/enhancement in solar wind pressure for either event and only small changes in the IMF orientation. Analysis of ACE and OMNI data showed a slight rotation in the Y-GSM IMF component for the 2002-08-10 event. However, we do not believe it significant enough to explain a sudden expansion of $\gtrsim$2 R_E near the bow shock nose. Analysis of the GOES data showed no evidence of a sudden change in pressure applied to the magnetosphere, thus no change in magnetopause/bow shock location. Given that these structures are observed > 60 c/ω_{pi} upstream of the last bow shock crossing, we also do not believe these features to be features of a reformation process [*e.g. Winske et al.*, 1990]. Therefore, we conclude that these structures are features of the terrestrial foreshock and not the bow shock.

Next, we needed to determine the local geometry of the bow shock. Figure 2 plots an overview of the magnetic field measurements observed for the two groups of shocklets and SLAMS. We will focus on the 2002-08-10 event herein. The blue line in Figures 2**E** and 2**J** represents the θ_{Bn} calculated from our first method and the magenta line was calculated using the second method, both discussed in Section 2. Note that the second method used a smoothed average magnetic field, instead of the HTR MFI data, and gaps indicate regions not magnetically connected to the model shock surface. The Rankine-Hugoniot solutions gave us shock normal vectors of $\sim$<+0.750, -0.621, -0.134> for the 2000-04-10 event and $\sim$<+0.987, -0.158, +0.002> for the 2002-08-10 event. We estimated the upstream foreshock average magnetic field, $\mathbf{B}_o$, using the Wind/MFI observations between 14:20-15:22 UT for the 2000-04-10 event and between 11:21-12:49 UT for the 2002-08-10 event. The average GSE vectors were found to be $\mathbf{B}_o \sim \langle +3.60, -2.99, -1.47 \rangle$ nT and $\sim \langle -4.32, +0.65, -0.41 \rangle$ nT, respectively. These estimates with the above shock normal vectors give $\theta_{Bn} \sim 14^\circ$ and $\sim 6^\circ$, respectively. Therefore, the Wind spacecraft was immersed within the quasi-parallel region of the terrestrial foreshock for the time of interest.

The foreshock structures, marked by vertical red lines in Figures 2**A**-**B** and 2**F**-**G**, were composed of a series of compressive magnetosonic waves (δB in phase with density, δn, fluctuations) identified as shocklets and SLAMS shown in Figures 2**C**-**D** and 2**H**-**I**, respectively. The SLAMS were observed to have: (1) mixtures of right- and left-hand polarizations (spacecraft frame); (2) very oblique ($\theta_{kB} \gtrsim 55^\circ$ and $\theta_{kV} \gtrsim 40^\circ$) propagation; and (3) $\delta B/B_o \gtrsim$ 2-6, consistent with previous observations [*Schwartz et al.*, 1992; *Wilkinson et al.*, 1993]. The 2002-08-10 event (Figure 2**H**-**I**) shows an isolated SLAMS near 12:52:20 UT. The 2000-04-10 event (Figure 2**C**-**D**) did not show a similar structure. The importance of this difference will be discussed in the next section.

Both groups of SLAMS have higher frequency fluctuations on their leading/upstream (i.e. the right-hand side of Figures 2**C**-**D** and 2**H**-**I**) edges, consistent with whistler mode waves. The characteristics of the waves immediately upstream(sunward) of the the steepened edges are consistent with previous observations of whistler precursors [*e.g. Wilson III et al.*, 2009]. The whistler amplitudes and beam intensity decrease away from the leading edge of the group of SLAMS and eventually the whistlers disappear when the FABs disappear. However, we cannot definitively show that the two phenomena are causally related because whistler modes have been observed in the absence of FABs. While simulations have found that reflected ions can provide free energy to enhance already present whistler precursors [*e.g. Scholer et al.*, 2003], supported by recent observations [*Wilson III et al.*, 2012], their primary source is thought to be dispersive radiation [*e.g. Sundkvist et al.*, 2012]. The source of the whistler mode waves are beyond the scope of this paper and we will not discuss them further.

3.2. Particle Distributions

We examined the effects caused by the series of shocklets and SLAMS on the ion and electron distribution functions for the two foreshock passes. The group of SLAMS created a rarefaction region behind the structures with a strong deflection of the solar wind core, analogous to the wake created by an obstacle in a fluid flow. The SLAMS caused strong anisotropic heating in the low energy ($\lesssim$1.1 keV) electrons and ions ($\lesssim$10 keV).

Figure 3 shows an example ion distribution (in the bulk flow frame) plotted as contours of constant phase space density versus velocity (axes range from $\pm$1500 km/s) containing a FAB. To aid the reader, we have inserted ellipses to show the location of the FAB (black) and solar wind beam (purple). In the top distribution, one can see the FAB (near $\sim$400 km/s) is moving anti-parallel to $\mathbf{B}_o$, which corresponds to the sunward direction for this event. Note that lowest energy bin for PESA High for both events was $\sim$80 eV (or $\sim$125 km/s proton). This figure is used for illustrative purposes and the format for all distributions shown in Figure 4 are consistent with the top contour plot in Figure 3. This distribution corresponds to panel **B** in Figure 4.

Figure 4 shows the HTR MFI data and select PESA High distribution functions for the time range corresponding to Figure 2**H**-**I**. The solar wind core is clearly identified in the center of sequential panels **S** to **AE** and separated from the FABs seen near $\sim$500-900 km/s in panels **S**-**AB** and $\sim$400 km/s in panel **B** (see Figure 3). The FAB in panel **B** is at lower speeds and comparison with foreshock distributions (*e.g.* panel **A**) improves contrast for better identification. The FABs on the downstream(earthward) side of the group of SLAMS are weaker for both events. Hot diffuse ions (i.e. nonthermal tail observed above $\sim$800 km/s) are observed continuously between 12:50:13 UT and 12:51:45 UT, simultaneous with the SLAMS. PESA Low and SWE distributions showed that the core ions experienced very strong heating in this region, strong enough to be observed by PESA High in panels **D**-**R** in Figure 4. The observed durations (Δt_{FAB}) of FABs and effects on core particle populations are consistent with previous observations [*Schwartz et al.*, 1992; *Wilkinson et al.*, 1993; *Meziane et al.*, 2004].

The FAB properties, summarized in the top half of Table 1, show the range of values found from our fit results. The values for the 2002-08-10 properties are for FABs observed between 12:51:51–12:52:48 UT and for FABs satisfying $V_b/V_A > 4$ (only one FAB had $V_b/V_A < 4$). These properties are consistent with previous observations upstream of the quasi-perpendicular bow shock [*e.g. Bale et al.*, 2005, *and references therein*]. The bottom half of Table 1 shows the instability analysis results. For reference, the magnetic field values used to produce the green arrows in Figure 1 correspond to $\Omega_{ci} \sim 0.44$ radians/s for the 2000-04-10 event and $\Omega_{ci} \sim 0.52$ radians/s for the 2002-08-10 event.

Note that FABs were observed both downstream(earthward) and upstream(sunward) of the group of SLAMS for both events (2000-04-10 event not shown). The FAB intensity was found to be greater on the upstream(sunward) side of the group of SLAMS but weaker on the upstream(sunward)

side of the isolated SLAMS (∼12:52:20 UT) shown in Figures 2**H**-**I**. Figure 5 shows a zoomed in view of the 2002-08-10 event where FABs are observed upstream(sunward) of the group of SLAMS. The timestamps for the data points were determined from the average of the start and end times of each PESA High distribution. One can see that n_b and n_b/n_o decrease until ∼12:52:15 UT then rise from ∼12:52:19 UT (Figure 4**W**) to ∼12:52:22 UT (Figure 4**X**). Note that the local peak at ∼12:52:22 UT corresponds to the ramp of the isolated SLAMS and that n_b and n_b/n_o decrease thereafter. The bottom two panels in Figure 5 show that V_b/V_{sw} and V_b/V_A increase steadily over this same interval.

The decrease in n_b/n_o with increasing distance upstream(sunward) from the group of SLAMS (shown in Figures 2**H**-**I**) suggests a local source. The large scale size (∼1000 km) and comparable gradient scale size (∼100 km) of SLAMS to the average ion inertial length (∼100 km) allows them to act as efficient magnetic mirrors when grouped together. Isolated SLAMS, however, are known to have lower amplitudes and thus lower phase speeds [*e.g. Schwartz et al.*, 1992], which results in a smaller velocity between incident solar wind ions and the SLAMS. The increase in n_b/n_o on the downstream side of the isolated SLAMS suggests that this structure is preventing some beam ions from escaping further upstream, consistent with previous observations [*Giacalone et al.*, 1993]. The local peak in n_b/n_o in the upstream(sunward) edge of the isolated SLAMS shows that it can reflect particles as well, but not as effectively as the group of SLAMS. The reasons for why an isolated SLAMS cannot reflect as well as the group of SLAMS may be: (1) isolated SLAMS are too narrow spatially; (2) they have smaller $\delta B/B_o$; (3) they do not propagate as fast causing their phase velocity relative to the bulk flow to be smaller; and/or (4) less rotation and turbulence in the magnetic field.

If the local magnetic field cannot connect the spacecraft with the bow shock without going through the group of SLAMS, then one would not expect to observe the coherent FABs shown in Figure 4. Therefore, if the group of SLAMS are between the spacecraft and the bow shock along an averaged magnetic field direction, then they must be the source of the FABs.

3.3. FAB Source

In this section we will explain why we believe the FABs originate from the SLAMS and not the bow shock. First we need to eliminate the possibility that the FABs produce the SLAMS by comparing observations to theory for ion/ion beam instabilities. Then we will use geometry to argue that the group of SLAMS create a magnetic barrier between the spacecraft and the bow shock. Lastly we will summarize our results and present our conclusions.

The observations show (Figures 2**C**-**D** and 2**H**-**I**) that the duration of individual SLAMS are longer for the 2002-08-10 event than the 2000-04-10 event. The predicted wave periods ($\omega_{rmax}{}^{-1}$) from Table 1 were ∼1.6-3.7s for the 2000-04-10 event and ∼5.4-25.1s for the 2002-08-10 event. The correspondence between the predicted wave periods and observed durations might initially suggest that the FABs are causing an ion/ion beam instability resulting in the observed SLAMS. However, this correspondence requires that the structures convect with the bulk flow and that they do not propagate in the plasma frame.

The average upstream(sunward) V_{sw} (∼460 km/s) is comparable for both events and the distribution of θ_{kV} are roughly the same. Therefore, we expect comparable Doppler effects for both events. Previous observations have shown that each individual SLAMS has a normal scale length L_n ∼ 1000 km and transverse scale length L_t ∼ 1300 km [*Lucek et al.*, 2008]. These scales correspond to convection time scales of L_n/V_{sw} ∼ 2.2 seconds per SLAMS and L_t/V_{sw} ∼ 2.8 seconds per SLAMS. These values do not seem to correlate with the observed wave periods, but we have ignored the phase speed of the SLAMS in these estimates.

Recall that the phase speed of SLAMS was determined to be V_{ph} ∼1-6 V_A [*Mann et al.*, 1994] and they are known to propagate nearly along the bow shock normal vector [*Lucek et al.*, 2008]. The geometry for both events is such that the spacecraft frame speed of the SLAMS is $V_o = |\mathbf{V}_{sw} + \mathbf{V}_{ph}| < V_{sw}$. For example, if we use $V_{ph} = 4\ V_A$ along the shock normal, then V_o ∼ 200-250 km/s for the 2000-04-10 event and V_o ∼ 80-230 km/s for the 2002-08-10 event. These new speeds change the convection time scales to L_n/V_o ∼ 4.1-5.0 seconds per SLAMS for the 2000-04-10 event and L_n/V_o ∼ 4.4-12.6 seconds per SLAMS for the 2002-08-10 event. Therefore, the longer observed durations for the SLAMS for the 2002-08-10 event can be explained by a slower convection speed of the structures.

Now we examine whether the beams could produce wave amplitudes large enough to match the observations. When we examined the parameters in Table 1 we used the results to estimate the saturation amplitude of the right-hand resonant and non-resonant ion/ion beam instabilities for $V_b/V_A \gg 1$ [*e.g. Gary*, 1991]. In this limit we find $\delta B/B_o \sim 0.4 \pm 0.1$ for the 2000-04-10 event and $\delta B/B_o \sim 1.3 \pm 0.1$ for the 2002-08-10 event. These values represent the mean plus or minus the standard deviation of the mean for all the beam distribution fit results for each event. Examination of the SLAMS in Figures 2**C**-**D** and 2**H**-**I** show $\delta B/B_o \sim$ 3-6, much larger than theory predicts. More importantly, the FABs are not observed inside the group of SLAMS. These results argue against the ion/ion beam instability as a source for the SLAMS.

Figure 6 is an illustrative cartoon that we will use to argue that the group of SLAMS, referred to as the obstacle for brevity, in each event is the source of the FABs. If we assume the obstacle is being convected with the solar wind at roughly $\mathbf{V}_{sw}$, then the spacecraft will be effectively stationary. Therefore, the path of the spacecraft through the obstacle is anti-parallel to $\mathbf{V}_{sw}$ with a length of $L_s = V_{sw}\ \Delta t_{sc}$. The amount of turbulence and rotation in the magnetic field observed through the obstacle should serve as a magnetic barrier from particles leaking into the upstream from behind the obstacle. Therefore, the spacecraft will be in the "magnetic shadow" of the obstacle, with respect to the terrestrial bow shock, for a distance L_{shadow}.

Recall that each individual SLAMS has scale lengths ∼ 1000 km. It takes Δt_{sc} ∼ 136s(108s) to traverse the obstacle and we observe FABs for Δt_{FAB} ∼ 10s(57s) for the 2000-04-10(2002-08-10) event. The duration the spacecraft spends within the obstacles (Δt_{sc}) suggests b ≪ a. The average complementary angle between $\mathbf{V}_{sw}$ and $\mathbf{B}_o$ is $< 25°$ for both events. Therefore, any trajectory through the obstacle above the horizontal in Figure 6 will result in the spacecraft being in the "magnetic shadow" of the obstacle for at least Δt_{sc} after exiting on the upstream(sunward) side.

If the spacecraft trajectory is below the horizontal in Figure 6 then we expect the duration in the "magnetic shadow" of the obstacle to be shorter than for trajectories above the horizontal. However, even for the trajectories resulting in significantly shorter durations of "magnetic shadow," the observations of FABs in such close proximity to the obstacle argues against a bow shock source.

4. Discussion and Conclusions

This study presents observations of field-aligned ion beams (FABs) near large amplitude magnetic field fluctuations in the terrestrial foreshock by the Wind spacecraft. We examined two foreshock events, on 2000-04-10 and 2002-08-10, composed of groups of shocklets and short large-amplitude magnetic structures (SLAMS). The 2002-08-10

event exhibited an isolated SLAMS upstream(sunward) of the group which allowed us to examine the evolution of the FAB through the structure.

The FABs propagate (in the plasma frame) away from the bow shock toward the upstream(sunward) side of the SLAMS. They had $T_b \sim$ 80-850 eV, $V_b/V_{sw} \sim$ 1.3-2.4, $T_{\perp,b}/T_{\parallel,b} \sim$ 1-8, and $n_b/n_o \sim$ 0.2-11%, consistent with previous observations [*e.g. Bale et al.*, 2005, *and references therein*]. While ion beams have been previously observed near SLAMS [*Schwartz et al.*, 1992; *Wilkinson et al.*, 1993], no previous reports have shown the evolution of ion distributions through SLAMS and showed the SLAMS to be the source of FABs.

We observed peak values of n_b/n_o near the upstream(sunward) edge of the group of SLAMS in both events. Another peak was observed on the immediate upstream(sunward) edge of the isolated SLAMS near 12:52:20 UT in the 2002-08-10 event. Just downstream(earthward) of the isolated SLAMS n_b/n_o increased suggesting the SLAMS was preventing beam ions from escaping upstream(sunward). The FABs for this event also had larger values of n_b, T_b, $T_{\perp,b}/T_{\parallel,b}$, and V_b/V_A. These differences are probably due to larger amplitude of the SLAMS in the 2002-08-10 event.

The source of the whistler precursors is beyond the scope of this manuscript. The SLAMS, however, are thought to be driven by gradients in the diffuse ion density [*e.g. Scholer et al.*, 2003]. We observed diffuse ions throughout each group of SLAMS and we did not observe FABs within either. Therefore, we believe the diffuse ions, not the FABs, are responsible for the SLAMS.

In summary, we argue that the SLAMS are the source of these FABs for the following reasons: (1) the decrease in n_b/n_o with increasing distance from the upstream(sunward) side of the group of SLAMS; (2) the evolution of the FABs across the isolated SLAMS shows a local peak in n_b/n_o on the immediate upstream(sunward) edge; (3) FABs are not observed within the group of SLAMS and their peak intensity is at the immediate upstream(sunward) edge of the group of SLAMS; (4) the predicted saturation amplitudes for the ion/ion beam instability are much smaller than observed; (5) observed differences in duration can be explained by differences in convection speed of the structures; and (6) geometry shows that the spacecraft is in the "magnetic shadow" of the group of SLAMS at the immediate upstream(sunward) edge. Therefore, at least the FABs observed immediately upstream(sunward) of the group of SLAMS cannot have a bow shock source and our results argue that it is likely the rest do not originate from the bow shock either.

The similarity of the field-aligned ion beams with those observed upstream of the quasi-perpendicular shock suggest the groups of SLAMS are acting like a local quasi-perpendicular shock. This is not to say that all field-aligned ion beams are produced by SLAMS. However, it is possible the beams are produced in a manner similar to those found in simulation results, showing a positive feedback loop between the waves and reflected particles [*e.g. Scholer and Burgess*, 1992].

In conclusion, we show the first direct evidence that groups of SLAMS can locally produce field-aligned ion beams.

Acknowledgments. We thank R. Lin (3DP), K. Ogilvie (SWE), and R. Lepping (MFI) for the use of data from their instruments. Data from ACE, GOES, Interball, and OMNI data were obtained from CDAWeb. All data sets from the Wind spacecraft were produced under Wind MO&DA grants. This research was supported by NESSF grant NNX07AU72H, grant NNX07AI05G, and the Dr. Leonard Burlaga/Arctowski Medal Fellowship.

References

Akimoto, K., D. Winske, S. P. Gary, and M. F. Thomsen (1993), Nonlinear evolution of electromagnetic ion beam instabilities, *J. Geophys. Res.*, *98*, 1419–1433, doi:10.1029/92JA02345.

Bale, S. D., et al. (2005), Quasi-perpendicular Shock Structure and Processes, *Space Sci. Rev.*, *118*, 161–203, doi:10.1007/s11214-005-3827-0.

Behlke, R., M. André, S. C. Buchert, A. Vaivads, A. I. Eriksson, E. A. Lucek, and A. Balogh (2003), Multi-point electric field measurements of Short Large-Amplitude Magnetic Structures (SLAMS) at the Earth's quasi-parallel bow shock, *Geophys. Res. Lett.*, *30*(4), 040,000–1, doi:10.1029/2002GL015871.

Blanco-Cano, X. (2010), Bow Shocks In The Solar Wind: Lessons Towards Understanding Interplanetary Shocks, *Twelfth International Solar Wind Conference*, *1216*, 459–465, doi:10.1063/1.3395903.

Bonifazi, C., and G. Moreno (1981a), Reflected and diffuse ions backstreaming from the earth's bow shock. I Basic properties, *J. Geophys. Res.*, *86*, 4397–4413, doi:10.1029/JA086iA06p04397.

Bonifazi, C., and G. Moreno (1981b), Reflected and diffuse ions backstreaming from the earth's bow shock 2. Origin, *J. Geophys. Res.*, *86*, 4405–4414, doi:10.1029/JA086iA06p04405.

Bougeret, J.-L., et al. (1995), Waves: The Radio and Plasma Wave Investigation on the Wind Spacecraft, *Space Sci. Rev.*, *71*, 231–263, doi:10.1007/BF00751331.

Briand, C. (2009), Review on electrostatic structures in the solar wind: observational considerations, *Nonlinear Proc. Geophys.*, *16*, 319–329.

Dubouloz, N., and M. Scholer (1995), Two-dimensional simulations of magnetic pulsations upstream of the Earth's bow shock, *J. Geophys. Res.*, *100*, 9461–9474, doi:10.1029/94JA03239.

Eastwood, J. P., E. A. Lucek, C. Mazelle, K. Meziane, Y. Narita, J. Pickett, and R. A. Treumann (2005), The Foreshock, *Space Sci. Rev.*, *118*, 41–94, doi:10.1007/s11214-005-3824-3.

Fuselier, S. A. (1995), Ion distributions in the Earth's foreshock upstream from the bow shock, *Adv. Space Res.*, *15*, 43–52, doi:10.1016/0273-1177(94)00083-D.

Fuselier, S. A., M. F. Thomsen, J. T. Gosling, S. J. Bame, and C. T. Russell (1986), Gyrating and intermediate ion distributions upstream from the earth's bow shock, *J. Geophys. Res.*, *91*, 91–99, doi:10.1029/JA091iA01p00091.

Gary, S. P. (1991), Electromagnetic ion/ion instabilities and their consequences in space plasmas - A review, *Space Sci. Rev.*, *56*, 373–415, doi:10.1007/BF00196632.

Giacalone, J., S. J. Schwartz, and D. Burgess (1993), Observations of suprathermal ions in association with SLAMS, *Geophys. Res. Lett.*, *20*, 149–152, doi:10.1029/93GL00067.

Gosling, J. T., J. R. Asbridge, S. J. Bame, G. Paschmann, and N. Sckopke (1978), Observations of two distinct populations of bow shock ions in the upstream solar wind, *Geophys. Res. Lett.*, *5*, 957–960, doi:10.1029/GL005i011p00957.

Gosling, J. T., M. F. Thomsen, S. J. Bame, W. C. Feldman, G. Paschmann, and N. Sckopke (1982), Evidence for specularly reflected ions upstream from the quasi-parallel bow shock, *Geophys. Res. Lett.*, *9*, 1333–1336, doi:10.1029/GL009i012p01333.

Greenstadt, E. W. (1976), Energies of backstreaming protons in the foreshock, *Geophys. Res. Lett.*, *3*, 553–556, doi:10.1029/GL003i009p00553.

Gurgiolo, C., G. K. Parks, B. H. Mauk, K. A. Anderson, R. P. Lin, H. Reme, and C. S. Lin (1981), Non-E x B ordered ion beams upstream of the earth's bow shock, *J. Geophys. Res.*, *86*, 4415–4424, doi:10.1029/JA086iA06p04415.

Hellinger, P., and A. Mangeney (1999), Electromagnetic ion beam instabilities: Oblique pulsations, *J. Geophys. Res.*, *104*, 4669–4680, doi:10.1029/1998JA900157.

Hoppe, M. M., and C. T. Russell (1983), Plasma rest frame frequencies and polarizations of the low-frequency upstream waves - ISEE 1 and 2 observations, *J. Geophys. Res.*, *88*, 2021–2027, doi:10.1029/JA088iA03p02021.

Hoppe, M. M., C. T. Russell, L. A. Frank, T. E. Eastman, and E. W. Greenstadt (1981), Upstream hydromagnetic waves and their association with backstreaming ion populations - ISEE 1 and 2 observations, *J. Geophys. Res.*, *86*, 4471–4492, doi:10.1029/JA086iA06p04471.

Kawano, H., S. M. Petrinec, C. T. Russell, and T. Higuchi (1999), Magnetopause shape determinations from measured position and estimated flaring angle, *J. Geophys. Res.*, *104*, 247–262, doi:10.1029/98JA02479.

Khrabrov, A. V., and B. U. Ö. Sonnerup (1998), Error estimates for minimum variance analysis, *J. Geophys. Res.*, *103*, 6641–6652, doi:10.1029/97JA03731.

Kis, A., M. Scholer, B. Klecker, H. Kucharek, E. A. Lucek, and H. Rème (2007), Scattering of field-aligned beam ions upstream of Earth's bow shock, *Ann. Geophys.*, *25*, 785–799.

Koval, A., and A. Szabo (2008), Modified "Rankine-Hugoniot" shock fitting technique: Simultaneous solution for shock normal and speed, *J. Geophys. Res.*, *113*, 10,110–+, doi:10.1029/2008JA013337.

Lepping, R. P., et al. (1995), The Wind Magnetic Field Investigation, *Space Sci. Rev.*, *71*, 207–229, doi:10.1007/BF00751330.

Lin, R. P., et al. (1995), A Three-Dimensional Plasma and Energetic Particle Investigation for the Wind Spacecraft, *Space Sci. Rev.*, *71*, 125–153, doi:10.1007/BF00751328.

Lucek, E., T. Horbury, A. Balogh, I. Dandouras, and H. Rème (2004), Cluster observations of structures at quasi-parallel bow shocks, *Ann. Geophys.*, *22*, 2309–2313.

Lucek, E. A., et al. (2002), Cluster magnetic field observations at a quasi-parallel bow shock, *Ann. Geophys.*, *20*, 1699–1710.

Lucek, E. A., T. S. Horbury, I. Dandouras, and H. Rème (2008), Cluster observations of the Earth's quasi-parallel bow shock, *J. Geophys. Res.*, *113*, 7–+, doi:10.1029/2007JA012756.

Mann, G., H. Luehr, and W. Baumjohann (1994), Statistical analysis of short large-amplitude magnetic field structures in the vicinity of the quasi-parallel bow shock, *J. Geophys. Res.*, *99*, 13,315–+, doi:10.1029/94JA00440.

Meziane, K., et al. (1997), Wind observation of gyrating-like ion distributions and low frequency waves upstream from the earth's bow shock, *Adv. Space Res.*, *20*, 703–706, doi:10.1016/S0273-1177(97)00459-6.

Meziane, K., C. Mazelle, R. P. Lin, D. LeQuéau, D. E. Larson, G. K. Parks, and R. P. Lepping (2001), Three-dimensional observations of gyrating ion distributions far upstream from the Earth's bow shock and their association with low-frequency waves, *J. Geophys. Res.*, *106*, 5731–5742, doi:10.1029/2000JA900079.

Meziane, K., et al. (2004), Simultaneous observations of field-aligned beams and gyrating ions in the terrestrial foreshock, *J. Geophys. Res.*, *109*, 5107–+, doi:10.1029/2003JA010374.

Meziane, K., A. M. Hamza, M. Wilber, C. Mazelle, and M. A. Lee (2011), Anomalous foreshock field-aligned beams observed by Cluster, *Ann. Geophys.*, *29*, 1967–1975, doi:10.5194/angeo-29-1967-2011.

Ogilvie, K. W., et al. (1995), SWE, A Comprehensive Plasma Instrument for the Wind Spacecraft, *Space Sci. Rev.*, *71*, 55–77, doi:10.1007/BF00751326.

Onsager, T. G., D. Winske, and M. F. Thomsen (1991), Interaction of a finite-length ion beam with a background plasma - Reflected ions at the quasi-parallel bow shock, *J. Geophys. Res.*, *96*, 1775–1788, doi:10.1029/90JA02008.

Paschmann, G., N. Sckopke, S. J. Bame, J. R. Asbridge, J. T. Gosling, C. T. Russell, and E. W. Greenstadt (1979), Association of low-frequency waves with suprathermal ions in the upstream solar wind, *Geophys. Res. Lett.*, *6*, 209–212, doi:10.1029/GL006i003p00209.

Paschmann, G., N. Sckopke, I. Papamastorakis, J. R. Asbridge, S. J. Bame, and J. T. Gosling (1981), Characteristics of reflected and diffuse ions upstream from the earth's bow shock, *J. Geophys. Res.*, *86*, 4355–4364, doi:10.1029/JA086iA06p04355.

Scholer, M., and D. Burgess (1992), The role of upstream waves in supercritical quasi-parallel shock re-formation, *J. Geophys. Res.*, *97*, 8319–8326, doi:10.1029/92JA00312.

Scholer, M., H. Kucharek, and I. Shinohara (2003), Short large-amplitude magnetic structures and whistler wave precursors in a full-particle quasi-parallel shock simulation, *J. Geophys. Res.*, *108*, 1273–+, doi:10.1029/2002JA009820.

Schwartz, S. J., and D. Burgess (1991), Quasi-parallel shocks - A patchwork of three-dimensional structures, *Geophys. Res. Lett.*, *18*, 373–376, doi:10.1029/91GL00138.

Schwartz, S. J., D. Burgess, W. P. Wilkinson, R. L. Kessel, M. Dunlop, and H. Luehr (1992), Observations of short large-amplitude magnetic structures at a quasi-parallel shock, *J. Geophys. Res.*, *97*, 4209–4227, doi:10.1029/91JA02581.

Slavin, J. A., and R. E. Holzer (1981), Solar wind flow about the terrestrial planets. I - Modeling bow shock position and shape, *J. Geophys. Res.*, *86*, 11,401–11,418, doi:10.1029/JA086iA13p11401.

Sundkvist, D., V. Krasnoselskikh, S. D. Bale, S. J. Schwartz, J. Soucek, and F. Mozer (2012), Dispersive Nature of High Mach Number Collisionless Plasma Shocks: Poynting Flux of Oblique Whistler Waves, *Phys. Rev. Lett.*, *108*, 025,002, doi:10.1103/PhysRevLett.108.025002.

Thomsen, M. F., J. T. Gosling, S. J. Bame, T. G. Onsager, and C. T. Russell (1990), Two-state ion heating at quasi-parallel shocks, *J. Geophys. Res.*, *95*, 6363–6374, doi:10.1029/JA095iA05p06363.

Tsubouchi, K., and B. Lembège (2004), Full particle simulations of short large-amplitude magnetic structures (SLAMS) in quasi-parallel shocks, *J. Geophys. Res.*, *109*, 2114–+, doi:10.1029/2003JA010014.

Wilkinson, W. P., A. K. Pardaens, S. J. Schwartz, D. Burgess, H. Luehr, R. L. Kessel, M. Dunlop, and C. J. Farrugia (1993), Nonthermal ions and associated magnetic field behavior at a quasi-parallel earth's bow shock, *J. Geophys. Res.*, *98*, 3889–3905, doi:10.1029/92JA01669.

Wilson III, L. B., C. A. Cattell, P. J. Kellogg, K. Goetz, K. Kersten, J. C. Kasper, A. Szabo, and K. Meziane (2009), Low-frequency whistler waves and shocklets observed at quasi-perpendicular interplanetary shocks, *J. Geophys. Res.*, *114*, 10,106–+, doi:10.1029/2009JA014376.

Wilson III, L. B., C. A. Cattell, P. J. Kellogg, K. Goetz, K. Kersten, J. C. Kasper, A. Szabo, and M. Wilber (2010), Large-amplitude electrostatic waves observed at a supercritical interplanetary shock, *J. Geophys. Res.*, *115*, 12,104–+, doi:10.1029/2010JA015332.

Wilson III, L. B., et al. (2012), Observations of Electromagnetic Whistler Precursors at Supercritical Interplanetary Shocks, *Geophys. Res. Lett.*, *39*, L08,109–+, doi:10.1029/2012GL051581.

Winske, D., V. A. Thomas, N. Omidi, and K. B. Quest (1990), Re-forming supercritical quasi-parallel shocks. II - Mechanism for wave generation and front re-formation, *J. Geophys. Res.*, *95*, 18,821–18,832, doi:10.1029/JA095iA11p18821.

Table 1. Instability Analysis Results

Range of Beam Parameters						
Date	T_b (eV)	$T_{\perp,b}/T_{\parallel,b}$	n_b/n_o (%)	V_b/V_{sw}	V_b/V_A	V_b/V_{Tb}
2000-04-10	80-170	1.1-4.4	0.2-1.6	1.5-2.0	7.5-8.5	3.7-5.0
2002-08-10	175-850	2.3-8.2	0.3-11.0	1.3-2.4	9.1-18.1	2.1-3.7
Instability Results						
Date	Δt_{FAB} (s)	γ_{max}/Ω_{ci}	$k_{max}\ V_A/\Omega_{ci}$		$\omega_{rmax}/\Omega_{ci}$	$\gamma_{max}{}^{-1}$ (s)
2000-04-10	∼10	0.10-0.20	0.18-0.32		0.34-1.43	9.10-19.6
2002-08-10	∼57	0.11-0.38	0.064-0.12		0.043-0.23	2.62-11.3

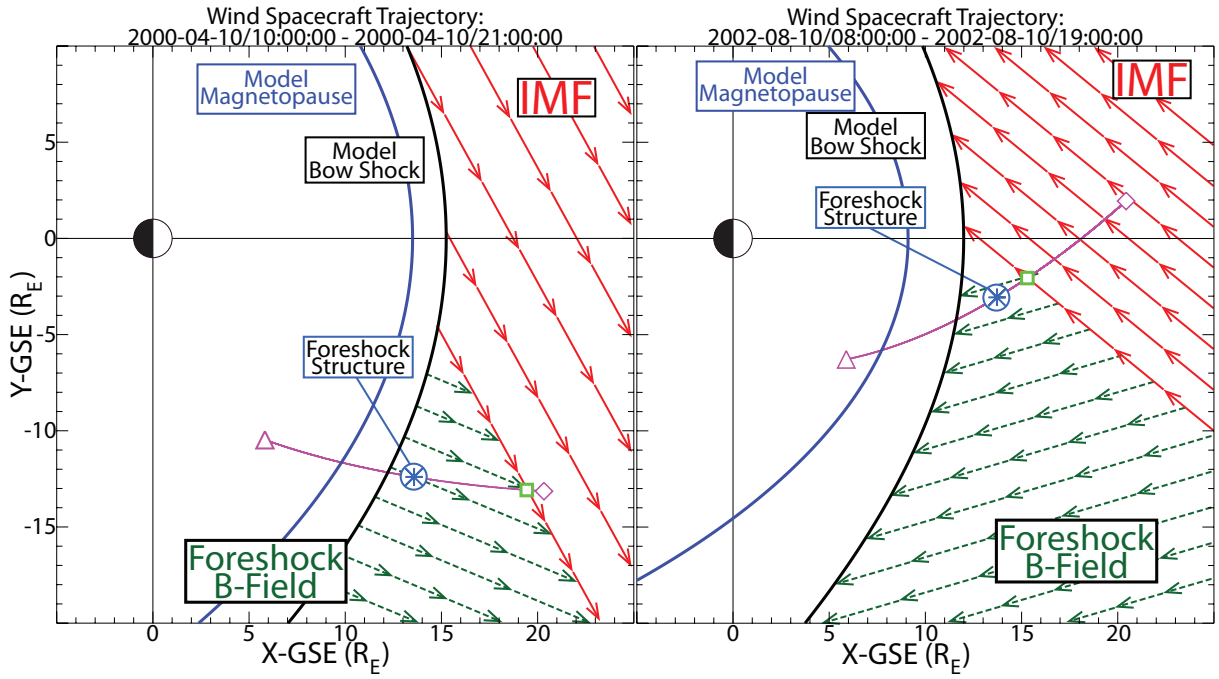

Figure 1. The trajectory (magenta line) of the Wind spacecraft in the XY-GSE plane for the 2000-04-10 (left panel) and 2002-08-10 (right panel) events. The triangle corresponds to the start time shown in the plot titles and the diamond the end time. The solid blue arc shows the projection of the model magnetopause location [*Kawano et al.*, 1999] and the solid black arc the model bow shock location [*Slavin and Holzer*, 1981]. The green arrows show the projection of the average magnetic field vector in the foreshock and the red arrows show the corresponding projection for the solar wind. The green square marks the approximate foreshock boundary location.

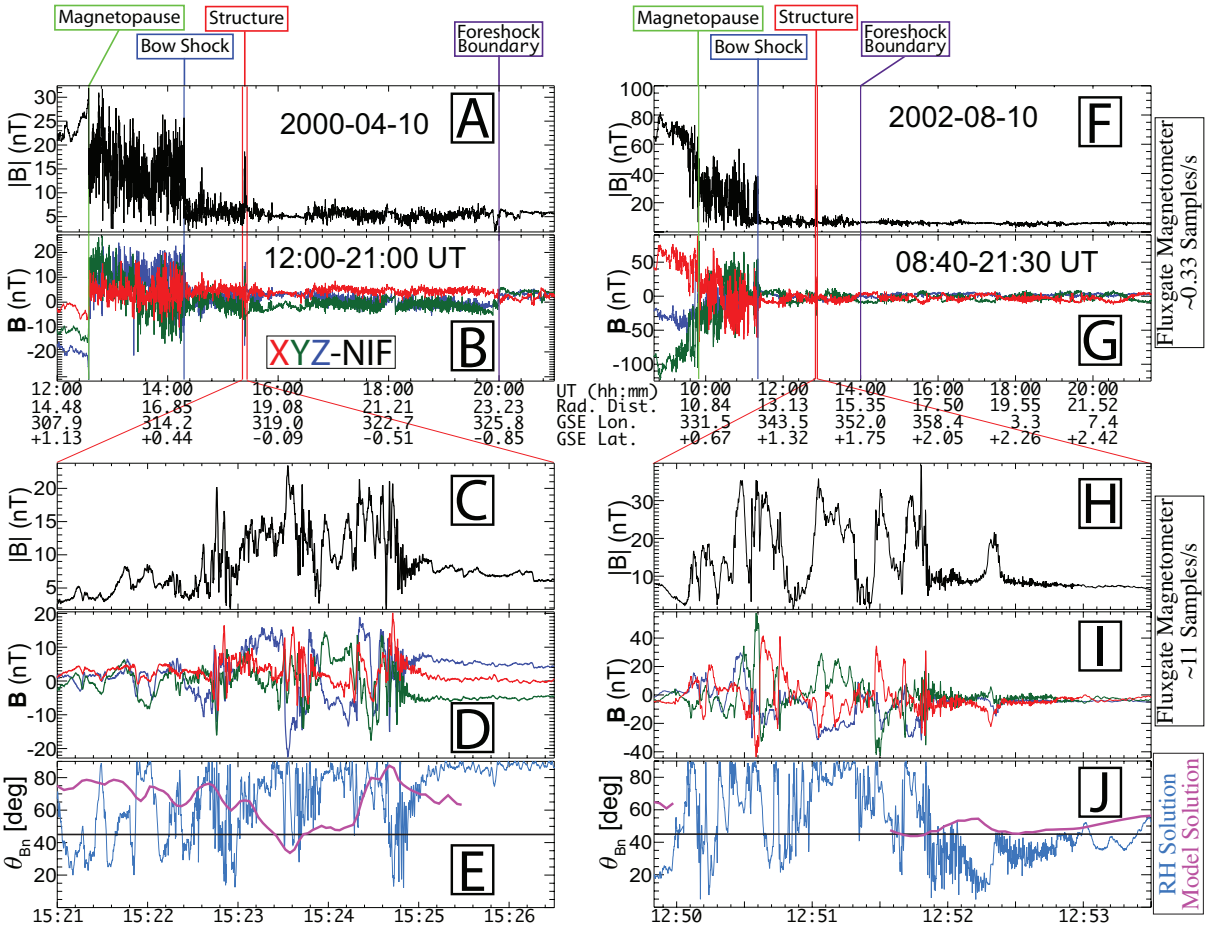

Figure 2. The top half of the figure shows three second resolution of the magnitude and the normal incidence frame (NIF) *Sundkvist et al.* [*e.g.* 2012] components of magnetic field data from the Wind spacecraft on 2000-04-10 (**A**-**B**) and 2002-08-10 (**F**-**G**) each with three vertical lines that indicate the magnetopause crossing (green), the last bow shock crossing (blue), the foreshock boundary (purple), and the red lines show the time periods for panels **C**-**E** and **H**-**J**. The tick mark labels at the bottom of these two panels are: UT time, and the Wind spacecraft radial distance (R_E), GSE longitude (degrees), and GSE latitude (degrees). Every panel has the same format, but the bottom two panels show the HTR MFI data and the shock normal angle for model (magenta) and Rankine-Hugoniot (blue) solutions.

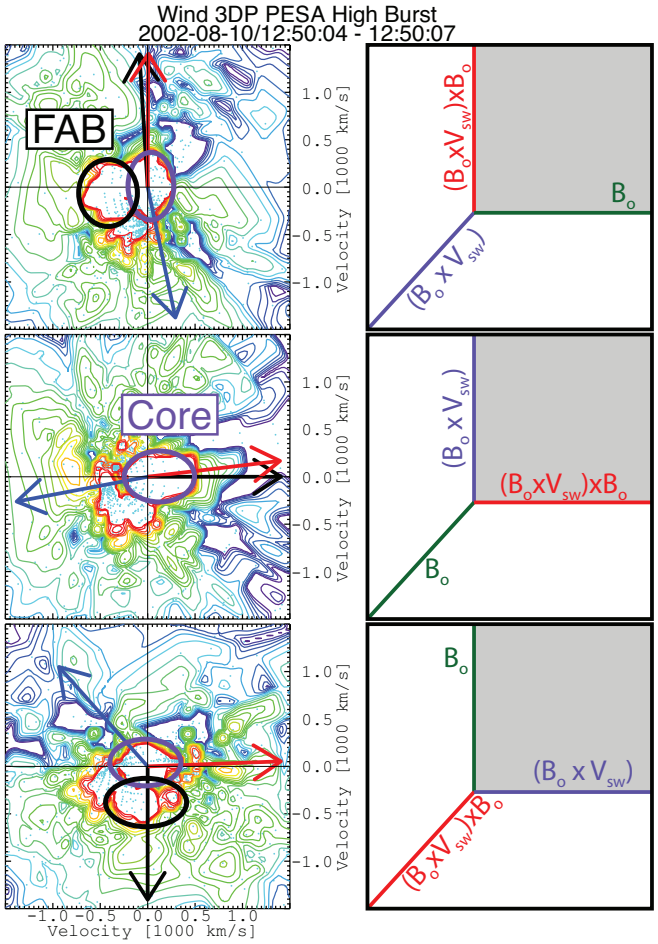

Figure 3. An example PESA High Burst distribution observed at 2002-08-10/12:50:04 UT. The contour plots show contours of constant phase space density (uniformly scaled from 1×10^{-13} to 1×10^{-9} $s^3cm^{-3}km^{-3}$, where red is high) projected onto three different planes defined by the shaded region in the coordinate axes shown in right-hand column. The diagonal axis defines the normal to the plane shown for each corresponding contour plot. Projected onto each contour are $\mathbf{V}_{sw}$ (black arrow), the sun direction (blue arrow), and the Earth direction (magenta arrow). The FAB (black ellipses) and core (purple ellipses) are labeled. This distribution corresponds to panel **B** in Figure 4.

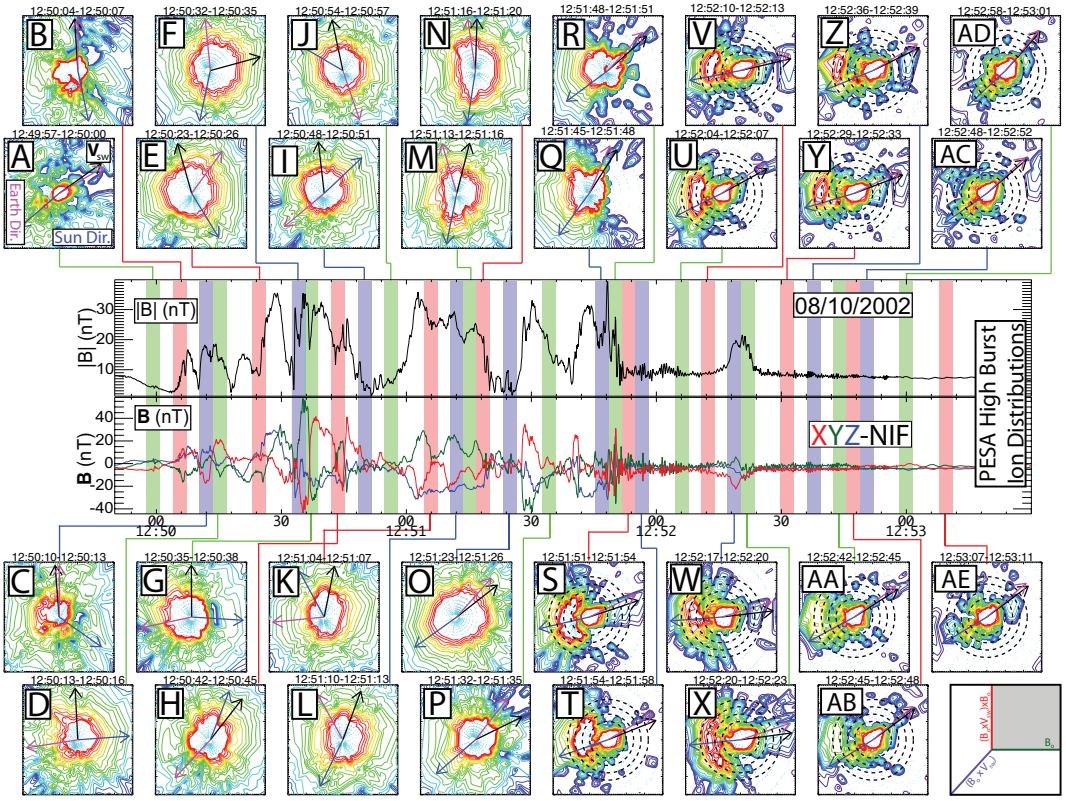

Figure 4. Selected PESA High Burst distributions shown for the time range shown in Figure 2**H-J**. The ion distribution plots are the same format as the top left panel of Figure 3. Panels **S-AE** have circles of constant energy at 500, 700, 900, and 1100 km/s. Ion beams are clearly identified in panels **B** and **S-AB**.

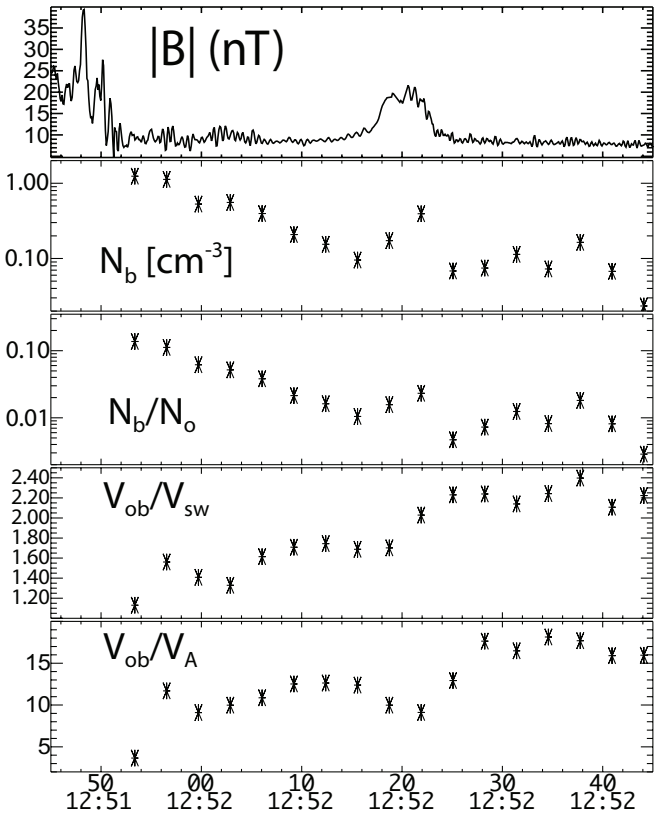

Figure 5. This figure shows the FAB parameters versus time with the magnitude of the magnetic field for the 2002-08-10 event. The panels, from top-to-bottom, show: magnetic field magnitude, B_o (nT); FAB number density, n_b (cm^{-3}); ratio of FAB to total number density, n_b/n_o; ratio of FAB drift speed to bulk flow speed, V_{ob}/V_{sw}; and ratio of FAB drift speed to local Alfvén speed, V_{ob}/V_A.

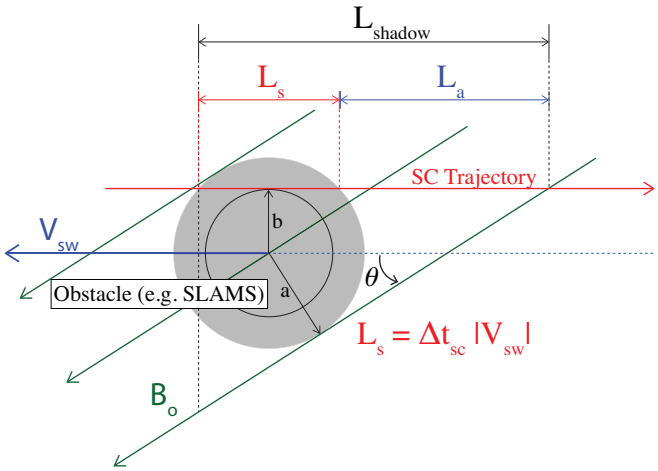

Figure 6. A schematic cartoon used to illustrate how the series of SLAMS in Figures 2**C-E** and 2**H-J** can block the spacecraft (SC) from "seeing" the bow shock along magnetic field lines. In this example, the sun is to the right and Earth to the left.